The effects of biliverdin on pressure-induced unfolding of apomyoglobin: The specific role of Zn2+ ions

Simeon Minic, Burkhard Annighöfer, Milos Milcic, François Maignen, Annie Brûlet, Sophie Combet

The effects of biliverdin on pressure-induced unfolding of apomyoglobin: the specific role of Zn^{2+} ions

Simeon MINIC[a,b,*], Burkhard ANNIGHÖFER[a], Milos MILCIC[c], François MAIGNEN[a], Annie BRÛLET[a], and Sophie COMBET[a,*]

[a]Laboratoire Léon-Brillouin (LLB), UMR12 CEA CNRS, Université Paris-Saclay, F-91191 Gif-sur-Yvette CEDEX, France ; [b]Center of Excellence for Molecular Food Sciences & Department of Biochemistry, University of Belgrade - Faculty of Chemistry, Belgrade, Serbia; [c]Department of General and Inorganic Chemistry, Faculty of Chemistry, University of Belgrade, Belgrade, Serbia.

[*]Corresponding authors: sminic@chem.bg.ac.rs ; sophie.combet@cea.fr

ABSTRACT

Apomyoglobin (apoMb), a model protein in biochemistry, exhibits a strong propensity to bind various ligands, which makes it a good candidate as a carrier of bioactive hydrophobic drugs. The stability of its hydrophobic pocket determines its potential as a carrier of bioactive compounds. High pressure (HP) is a potent tool for studying protein stability, revealing the specific role of hydrophobic cavities in unfolding. We probed the effects of biliverdin (BV) binding and its complex with Zn^{2+} ions on the structure and HP stability of apoMb. CD spectroscopy and SAXS measurements revealed that BV and BV-Zn^{2+} complexes make the apoMb structure more compact with higher α-helical content. We performed *in-situ* HP measurements of apoMb intrinsic fluorescence to demonstrate the ability of BV to stabilise apoMb structure at HP conditions. Furthermore, the presence of Zn^{2+} within the apoMb-BV complex significantly enhances the BV stabilisation effect. *In-situ* visible absorption study of BV chromophore confirmed the ability of Zn^{2+} to increase the stability of apoMb-BV complex under HP: the onset of complex dissociation is shifted by ~100 MPa in the presence of Zn^{2+}. By combining HP-fluorescence and HP-visible absorption spectroscopy, our strategy highlights the crucial role of tetrapyrrole-metal complexes in stabilising apoMb hydrophobic pocket.

Keywords: Apomyoglobin, Biliverdin, High-pressure, Binding, Zinc, Stability

INTRODUCTION

Myoglobin (Mb), a globular, α-helicoidal, and monomeric protein, is one of the most studied and best-characterised proteins. The prominent structural feature of Mb is the binding pocket which accommodates the heme prosthetic group responsible for the oxygen binding and its storage in the muscle [1, 2]. Apomyoglobin (apoMb; Fig. 1), obtained by heme removal from Mb, has long been used as a paradigm in kinetic and thermodynamic studies of protein folding and dynamics [3]. Indeed, the protein forms many partly folded states of varying compactness and secondary structure content that can be studied at equilibrium, providing insights into its folding landscape [4]. ApoMb exhibits significant similarity with holomyoglobin (holoMb) regarding the protein secondary structure and overall conformation. However, compared to the holoprotein, apoMb is less compact, has slightly lower α-helical content, and exhibits a significantly reduced thermodynamic stability [3].

Heme binding site in apoMb can accommodate various heme analogues, usually complexed with metal ions, giving them strong bioactive effects [1, 5, 6]. However, bioactive heme analogues in free form exhibit poor water solubility and their incorporation in well-characterised stable proteins are required for efficient drug delivery [5]. Designing structurally and functionally stable proteins are crucial for medical applications and laboratory-based research, as a slight deviation in surrounding condition from their original cellular environment may lead to their denaturation and then may destroy their biological functionality [7]. Therefore, the primary prerequisite for the successful application of apoMb as a drug carrier is the stability of its binding pocket, enabling the successful delivery of bioactive molecules. In this respect, probing the stability of the heme-binding pocket in apoMb in presence and in absence of ligands could give significant insights into the potential of apoMb as a drug carrier. In order to test the stability of apoMb-binding complexes, one can use high pressure (HP). It is an excellent tool for studying the stability of binding pockets within the protein structure due to the ability of pressure to eliminate the hydrophobic cavities present in the folded state of proteins [8]. Moreover, several studies demonstrate the ability of ligands to increase the

compactness and stabilise internal protein cavities at HP conditions, contributing to the high pressure stability of proteins [9-11]. Hence, it is crucial that ApoMb-binding bioactive molecules can stabilise the protein structure, increasing the potential of ApoMb as a drug carrier.

The tetrapyrrole-based ligands exhibit various bioactive effects and interesting physicochemical properties, giving them the significant potential for application in medicine and biotechnology [5, 12, 13]. For example, their ability to absorb light at long wavelengths, as well as to bind various metal ions, makes them great candidates for applications in photodynamic therapy, optogenetics and optochemistry [14-16]. Biliverdin (BV) (Fig. 1), one of the best-studied tetrapyrroles, is not only a metabolic product of heme metabolism but also a molecule with significant bioactive properties [17], and a photoreceptor role in bacterial phytochromes [14]. Its conformational flexibility enables it to interact with various proteins, including apoMb (Fig. 1), albumin, and lipocalin-type prostaglandin D synthase [18-20]. Furthermore, the ability of BV to complex physiologically relevant metal ions, such as zinc (Zn^{2+}) and copper (Cu^{2+}), further highlights its physiological relevance [15, 21].

Therefore, considering *i*) the propensity of apoMb to bind various ligands [5, 6, 19, 22-24], *ii*) the bioactive properties of tetrapyrrole-metal complexes, and *iii*) the heme-binding pocket of apoMb as its essential structural feature, we consider BV-Zn^{2+} complex as an excellent model system for binding apoMb and improving its stability. The findings obtained from studying this model system could give significant insights into the role of hydrophobic cavities in the stability of apoMb-bioactive tetrapyrrole-based ligands complexes, which could improve the potential of apoMb as a drug carrier. The present work aims to study the impact of BV and BV-Zn^{2+} complexes on apoMb structure and its stability under HP. We employed a protein fluorescence quenching and molecular docking approaches to demonstrate and compare the binding of BV and BV-Zn^{2+} complex to apoMb. We show by CD spectroscopy and small-angle X-ray scattering (SAXS) measurements that BV binding, either in presence, or in absence of Zn^{2+} ions, makes the protein structure more compact compared to its free form. *In situ* HP measurements of apoMb intrinsic fluorescence demonstrates the ability of

BV to significantly increase the pressure stability of apoMb, while the presence of Zn^{2+} enhances BV stabilisation effect. Furthermore, *in situ* HP visible (VIS) measurements of BV and BV-Zn^{2+} complex in presence of apoMb confirm the HP stability of apoMb-BV-Zn^{2+} complex in comparison to apoMb-BV in absence of Zn^{2+} ions.

MATERIALS & METHODS

Materials

Myoglobin (Mb, 17 kDa) from the equine heart was purchased from Sigma-Aldrich (USA) and the heme group was removed by the acid/butanone method [25]. Obtained apoMb was extensively dialysed against water, and its concentration was determined from the extinction coefficient of 15.9 mM^{-1} cm^{-1} at 280 nm [26]. All experiments were performed by diluting a dialysed stock solution of apoMb in 100 mM MES buffer, pH 6.0, at 20°C. BV was purchased from Sigma-Aldrich (USA) and solubilised in DMSO with concentrations not exceeding 5% (*v*/*v*). All other chemicals were of analytical reagent grade, and Milli-*Q* water was used as a solvent.

Determination of BV binding constant to apoMb

The binding of BV to apoMb was studied by the fluorescence quenching titration method, using the intrinsic fluorescence of apoMb as a probe at constant protein concentration (1 μM) and various BV concentrations (0.05 to 6.4 μM). All measurements were performed on the Cary Eclipse fluorescence spectrometer (Varian, USA). The protein was also titrated with the mixture of BV and Zn^{2+} ions to achieve the final concentrations of BV and Zn^{2+} in the range of 0.05 to 6.4 μM and 0.5 to 64 μM, respectively. The concentration of Zn^{2+} was kept ten times higher than the BV concentration to assure the saturation of the BV chromophore with the metal ion. The excitation wavelength was set at 280 nm (excitation of both Trp and Tyr), and the emission spectra were read from 300 to 400 nm. The ability of BV to absorb at excitation and emission wavelengths decreases apoMb fluorescence, which may lead to wrong interpretation of the binding results. Therefore, fluorescence intensities of apoMb were corrected for the inner-filter effect arising from the ability of BV to absorb the excited light and the re-absorb the emitted light, according to the following equation [27]:

$$F_c = F_0 10^{(A_{em}+A_{ex})/2} \qquad \textbf{(1)}$$

where F_0 is the measured fluorescence, F_c is the corrected fluorescence, and A_{ex} and A_{em} are the absorbance of BV at excitation (280 nm) and peak emission (333 nm) wavelength, respectively.

To determine the type of quenching, Stern–Volmer's (SV) constants were calculated using the equation [27]:

$$\frac{F_0}{F} = 1 + K_{\mathrm{SV}}[\mathrm{BV}] = 1 + k_{\mathrm{q}}\tau_0[\mathrm{BV}] \qquad \textbf{(2)}$$

where F_0 and F are protein fluorescence intensities at 333 nm in absence and presence of ligand, respectively, k_q is the quenching rate constant of the biomolecule, τ_o is the average lifetime of the apoMb without quencher (2.5 ns) [28], [BV] is BV concentration, and K_{SV} is SV quenching constant. The estimation of the apparent dissociation constant ($K_d{}^{app}$) of the apoMb-BV system was done using the equation [29]:

$$\frac{F_0 - F}{F_0} = \frac{A[BV]}{K_d{}^{app} + [BV]} \qquad \textbf{(3)}$$

where A is the coefficient which denotes the maximal apoMb fluorescence quenching ($F \rightarrow 0$): for fitting purposes, A was kept constant at 1, representing the saturation of apoMb with BV. The apparent binding constant ($K_a{}^{app}$) is equal to the reverse value of $K_d{}^{app}$. It should be emphasised that original equation 3 comprises the concentration of free ligand concentration. However, in this study, we use the total concentration of BV in equation 3 because the high affinity of BV to apoMb (K_d far below 1 μM) disables the precise determination of free BV concentration. In this context, the obtained binding/dissociation constants are declared as apparent.

Molecular docking

For molecular docking experiment, crystal structure of apoMb in complex with biliverdin (PDB ID: 1BVC) [30] was extracted from the Protein Data Bank and all heteroatoms (BV, phosphate ions, and water molecules) were removed from this structure. The obtained structure of apoMb was used for molecular docking of BV and BV-Zn^{2+} complex. The docking was done with Auto Dock 4.2 [31] program. The structure optimisation procedure of the BV-Zn^{2+} complex structure (Fig. 1B) is given in the Supplementary Information (SI).

CD spectroscopy measurements

CD measurements were carried out on a Chirascan spectropolarimeter (Applied Photophysics, UK) under constant nitrogen flow. Spectra of 10 µM apoMb in absence and presence of BV or BV-Zn^{2+} complex (10 µM BV and 100 µM Zn^{2+}) were recorded in the range of 200–250 nm at a scan speed of 50 nm/min, using a cell with an optical pathlength of 2 mm. Buffer and ligand spectra were subtracted from the spectra of apoMb and apoMb-ligand complexes, respectively. Mean residue ellipticity (MRE) was calculated from equation [32]:

$$MRE = \frac{\theta}{10rl[apoMb]} \qquad \textbf{(4)}$$

where θ is the ellipticity in mdeg at 222 nm, r the number of amino acid residues of apoMb (154), l the pathlength of the cell in cm (0.2), and [apoMb] the molar concentration of the protein.

The α-helical content of free and bound apoMb was calculated from MRE values at 222 nm using the following equation [33]:

$$\%\,\alpha - helix = \frac{-MRE_{222\,nm} - 3{,}000}{39{,}500 - 3{,}000} \qquad \textbf{(5)}$$

For the comparison of α-helical content between different samples, an analysis of variance (ANOVA) of data was performed, and means comparisons were made using the Tukey test.

Small-angle X-ray (SAXS) scattering measurements

In order to study the effects of BV and BV-Zn^{2+} complex on the tertiary structure of apoMb, we performed small-angle X-ray scattering (SAXS) measurements. SAXS experiments were carried out on the Xeuss 2.0 apparatus (Xenocs, France) of LLB (SWAXS Lab, CEA-Saclay, France). The instrument uses a microfocused CuKa source (wavelength of 1.54 Å, 8 keV) and a Pilatus3 1 M detector (Dectris, Switzerland). One sample-to-detector distance (SD = 54 cm) was chosen to cover a Q-range extending from 0.025 to 0.38 $Å^{-1}$, with a beam size of 1.2 x 1.2 mm^2 (entrance) and 0.8 x 0.8 mm^2 (exit). Solutions of apoMb (235 µM, 4 g/L) in absence and presence of BV (235 µM) or BV-Zn^{2+} complex (235 µM both) were put in Kapton capillaries. Measurements of buffer, empty

capillary, empty beam, and electronic background ("dark") were subtracted according to the procedure previously established for small-angle neutron scattering (SANS) [34]. Scattering data normalised to the transmitted X-ray beam and sample thickness (0.145 cm) are in cm^{-1}.

SAXS data analysis

The classical expression of the scattering intensity $I(Q)$ (in cm^{-1}) of centrosymmetric and relatively monodisperse particles can be written:

$$I(Q) = n\,\Delta\rho^2\,V_{\text{part.}}^2\;P(Q)\,S(Q) \qquad \textbf{(6)}$$

where n is the number of particles *per* unit volume (cm^{-3}), $\Delta\rho$ (contrast) the difference in the X-ray scattering length density between the particles and the solvent (cm^{-2}), and $V_{\text{part.}}$ (cm^3) the specific volume of each particle. The form factor $P(Q)$ describes the shape of the particles and fulfils the condition $P(0) = 1$, while the structure factor $S(Q)$ describes the interactions between the particles. In absence of interactions, like in a dilute solution, $S(Q) = 1$. The SAXS intensity curves of apoMb, either in presence, or in absence of ligands (Fig. 3B), indicate protein partial aggregation. Therefore, SAXS curves were fitted by a sum two intensity profiles using SasView software (https://www.sasview.org):

a) *the scattering profile of a sphere with uniform scattering length density (SLD) corresponding to the apoMb globular shape [35]:*

$$I_{sph}(Q) = \frac{A_{sph}}{V} * [3V(\Delta\rho) * \frac{\sin(Qr) - Qr\cos(Qr))}{(Qr)^3}]^2 \qquad \textbf{(7)}$$

where A_{sph} is a constant that corresponds to the volume fraction of the sample occupied by the spheres and V and r are the volume and radius of the spheres, respectively. $\Delta\rho$ is the difference between the SLDs of the scatterer and the solvent.

b) *A power law representing the scattering of aggregates at low Q:*

$$I_{agg}(q) = A_{agg} * Q^{-\alpha} \qquad \textbf{(8)}$$

where α represents the power law exponent and A_{agg} is a constant without physical significance.

The fitting procedure of the scattered intensity *I(Q)* is done by the expression:

$$I(Q) = I_{sph} + I_{agg} + background \qquad \textbf{(9)}$$

where *background* represents the *Q*-independent level of noise.

The procedure is justified *a posteriori* by the relatively small contribution of $I_{agg}(Q)$ to the total intensity (Table S1). The fitted value of the exponent α is phenomenological, due to the restricted domain of *Q* where its effect can be observed.

The Primus software [36] was used to determine the radius of gyration (R_g) of apoMb in presence and absence of ligands. These values are defined at small *Q*-values (QR_g < 0.4-1.3) by the Guinier approximation with [35]:

$$\ln\left(\frac{I(Q)}{I(0)}\right) = -\frac{Q^2 {R_g}^2}{3} \qquad \textbf{(10)}$$

HP-fluorescence measurements and analysis

Fluorescence measurements at HP conditions were performed on an SLM 8,000 fluorescence spectrometer (USA) using HP optical bomb with optically flat sapphire windows and a HP generator, as previously described [37]. A square quartz cell (with an optical pathlength of 5 mm) containing the sample was positioned within the HP optical bomb, while a plastic membrane on the top of the cell separated the sample from the pressure-transmitting liquid (H_2O).

Fluorescence spectra of apoMb solution (10 μM) in absence and presence of BV (10 μM) or BV-Zn^{2+} complex (10 μM BV, 100 μM Zn^{2+}) were recorded between 320 and 365 nm, with a data interval of 0.2 nm and an excitation wavelength of 280 nm, at a scanning speed of 10 nm/min. Excitation and emission slits were set to 4 and 8 nm, respectively. Spectra were recorded at various pressures between 0.1 and 380 MPa, with steps of 10 or 30 MPa. The pressure was increased at a rate of 10 MPa/min. After each pressure change, a delay of 2 min was taken prior to the measurements, in order

to reach equilibrium. The obtained spectra were smoothed using a Savitzky-Golay algorithm with 100 points of the window. Unfolding curves were obtained by studying the dependence of wavelength of emission maxima on pressure, normalised for the fluorescence intensity at each corresponding pressure point, according to the equation:

$$Y = \frac{\lambda_P - \lambda_{atm}}{\lambda_{Pmax} - \lambda_{atm}} * \frac{F_P}{F_{Pmax}} \qquad \textbf{(11)}$$

where λ_{atm}, λ_{Pmax}, and λ_P represent the emission maximum at the atmospheric pressure, at the highest pressure, and pressure P, respectively. F and F_{Pmax} represent the fluorescence intensity at emission maximum at pressure P and the highest pressure, respectively. In order to calculate the percentage of apoMb unfolding, Y values obtained in Eq. 11 are normalised according to the equation:

$$\%_{apoMb\ unfolding} = \frac{Y_P - Y_{atm}}{Y_{Pmax} - Y_{atm}} * 100 \qquad \textbf{(12)}$$

The Gibbs free energy change at 0.1 MPa ($\Delta G_{0.1\ \mathrm{MPa}}$) and the apparent volume change (ΔV_u) due to protein unfolding were determined by fitting the pressure denaturation curves with the following equation adapted from [38], by replacing A_l and A_h amplitudes by 0 and 100, respectively.

$$\%_{apoMb\ unfolding} = 100 - \frac{100}{1 + e^{-\frac{\Delta G_{0.1\ MPa} + \Delta V u * P}{RT}}} \qquad \textbf{(13)}$$

The pressure at which one-half (50%) of the protein is unfolded defines the half-denaturation pressure ($P_{1/2}$). The percentage of unfolding, obtained from Eq. 12, is used to fit the unfolding curves as a function of pressure in Eq. 13, which allows getting both $\Delta G_{0.1\ \mathrm{MPa}}$ and ΔV_{u}.

HP-VIS absorption measurements and analysis

Visible (VIS) absorption spectra at HP conditions were recorded on a Cary 3E spectrometer (Varian, USA) using HP optical bomb with sapphire windows and a HP generator, as previously described [9, 39]. A square quartz cell (with an optical pathlength of 5 mm) containing the sample was positioned within the HP optical bomb, while a plastic membrane on the top of the cell separates the sample

from the pressure-transmitting liquid (H_2O). VIS spectra of apoMb-BV mixture (80 µM both) in presence and absence of 80 µM Zn^{2+} were recorded between 500 and 900 nm, with a bandwidth of 1 nm and a data interval of 0.5 nm, at a scanning speed of 150 nm/min. Spectra were recorded at various pressures between 0.1 and 300 MPa, with steps of 30 MPa. The pressure was increased at a rate of 10 MPa/min. After each pressure change, a delay of 2 min was taken prior to the measurements, in order to reach equilibrium. Measurements of buffer solution were performed under the same conditions. The recorded spectra were subtracted from the spectra of apoMb-BV and apoMb-BV-Zn^{2+} complexes. The dissociation of protein-ligand complexes as a function of the pressure P is quantified according to the equation:

$$Y = \frac{Abs_{free\ BV}}{Abs_{bound\ BV}} \qquad \textbf{(14)}$$

Where $Abs_{free\ BV}$ represents the intensity of the absorption peak arising from dissociated BV (averaged absorbances in the range 660-665 nm), while $Abs_{bound\ BV}$ is the intensity of the absorption peak of BV bound to apoMb in absence (averaged absorbances in the range 700-705 nm) or in presence of Zn^{2+} (averaged absorbances in the range 815-820 nm). In order to calculate the percentage of apoMb dissociation, Y values obtained in Eq. 14 are normalised according to Eq. 12. The Gibbs free energy change at 0.1 MPa ($\Delta_{G01\ MPa}$) and the apparent volume change (ΔV_u) due to BV dissociation were determined as described above (Eq. 14).

RESULTS

Binding of BV and BV-Zn^{2+} complex to apoMb

The presence of two tryptophan residues in apoMb induces strong protein emission upon excitation at 280 nm. The addition of BV (Fig. S1) and BV-Zn^{2+} complex (Fig. S2) in gradually increasing concentrations induces a significant quenching of apoMb fluorescence. On the other hand, adding Zn^{2+} in absence of BV did not produce any significant quenching of apoMb fluorescence (data not

shown). In general, there are two types of quenching: static (contact) and collisional ones. The obtained Stern-Volmer quenching constants (Fig. 2A) of 2.9±0.2 x 10^6 M^{-1} (BV) and 3.3±0.1 x 10^6 M^{-1} (BV-Zn^{2+} complex) are used to calculate bimolecular quenching rate constants for BV (1.2±0.1 x 10^{15} $M^{-1}s^{-1}$) and BV-Zn^{2+} complex (1.3±0.1 x 10^{15} $M^{-1}s^{-1}$). Considering that the bimolecular quenching rate constant in both cases is five orders of magnitude higher than the diffusion rates of biomolecules (10^{10} $M^{-1}s^{-1}$) [40], these data indicate that static (contact) quenching of apoMb fluorescence occurs. Moreover, a significant change in the BV absorption spectrum in presence of apoMb (see below) confirms the formation of a stable protein-ligand complex. Indeed, based on apoMb fluorescence spectra, we obtained strong apparent binding affinities K_a^{app} (equation 3; Fig. 2B) of BV to apoMb (2.4 ±0.2 x 10^6 M^{-1}), while the presence of Zn^{2+} ions increases the BV apparent binding affinity to 3.2±0.2 x 10^6 M^{-1}.

Molecular docking of BV and BV-Zn^{2+} complex to apoMb

As detailed above and in the SI, BV molecule was removed from the crystal structure of apoMb:BV complex (PDB: 1BVC). In order to verify the method, redocking experiments of neutral and anionic forms of BV to apoMb were performed. Both ligands bind to athe heme binding pocket of apoMb with a root mean square deviation (RMSD) from the crystal structure less than 0.5 Å (Fig. S3). The main interaction between pyrrole rings of BV and protein residues are π-π stacking (Phe138 and Phe43), π-π T-shaped (His64), and π-sigma (Val68). Also, Ser92 and His97 are involved in hydrogen bonding with the carboxylic group from BV (Fig. S4).

The best binding site for BV-Zn^{2+} complex, found from the docking experiment, is in the same binding pocket as for BV alone (Fig. 1, A & C). The structure of the complex is slightly rotated compared to BV structure, inducing different interactions with amino-acids. π-π stacking interactions are now formed between complex pyrrole rings and His97 and Phe43, π-π T-shaped with His64, while His97 and Lys42 are also involved in hydrogen bonding with complex carboxylic groups (Fig. S5). Furthermore, nitrogen atoms from His93 and His64 are in the close proximity to the zinc (II) ion

(3.1 Å and 4.0 Å, respectively) and are properly oriented for the formation of coordination bond (Fig. S6).

Structural changes of apoMb in presence of BV or BV-Zn^{2+} complex

Far-UV CD spectrum of apoMb at pH 6.0 shows negative ellipticity between 200 and 250 nm, with two minima at 208 and 222 nm (Fig. 3A), which is a typical characteristic of α-helical proteins. The presence of BV or BV-Zn^{2+} complex increases the negative ellipticity of apoMb. Based on the ellipticity at 222 nm, we calculated the α-helical content of apoMb, which increases upon adding BV or BV-Zn^{2+} complex by 6-7% (Table 1). Furthermore, the addition of ligands induces the changes in the shape of the far-UV CD spectrum of apoMb through the increase of 222 nm/208 nm ellipticity ratio (Table 1), while the BV-Zn^{2+} complex has a slightly more pronounced effect in comparison to free BV. Therefore, an increase in the 222 nm/208 nm ellipticity ratio indicates the induction of α-helical coiled-coil secondary structures upon ligand addition [40].

SAXS measurements were performed to evaluate the effects of BV and BV-Zn^{2+} complex on apoMb tertiary structure. SAXS profiles, obtained before and after the subtraction of a power law contribution are shown in Figs. 3B and 3C, respectively. We attribute the power law at low Q to the presence of aggregates. The Q-domain covered by the experiment only allows us to see the beginning of the rise of $I(Q)$ at the smallest values of Q, which explains the relatively small absolute value of the exponent of the power law. We validated that this subtraction approach is correct by fitting the subtracted curve of the apoMb-BV complex (Fig. 3C) with the theoretical curve of apoMb-BV crystal structure (Fig. S7) using CRYSOL software (ATSAS). The presence of ligands has a discrete effect on the plot intensity in the Q-range of 0.1-0.2 $Å^{-1}$ in comparison to free apoMb, and the SAXS spectra of apoMb in presence of BV or BV-Zn^{2+} complex are mainly superimposed (Fig. 3B). Radii of gyration values (R_g), obtained from Guinier plots, indicate that the presence of BV or BV-Zn^{2+} complex induces a higher compactness of apoMb in comparison to its free form. Additionally, SAXS

intensities were fitted by the sphere form factor (Fig. 3C, Table 1) and the obtained sphere radius and volum of apoMb decreases in presence of ligands.

Table 1. The effects of BV and BV-Zn^{2+} complex on apoMb secondary (CD spectroscopy) and tertiary (SAXS) structures at pH 6.0.

Samples	CD spectroscopy		SAXS			
	α-helix (%)	$\theta_{222\ nm}/\theta_{208\ nm}$ (x 100)	[a]R_g (Å)	[b]R (Å)	[b]V (10^3 x Å^3)	[b]χ^2
apoMb	62±1[1]	93±1[1]	18.3±0.3	21.8±0.1	43.4±0.1	2.96
apoMb-BV	69±1[2]	99±1[2]	15.2±0.2	19.5±0.1	31.0±0.1	2.34
apoMb-BV-Zn^{2+}	69±1[2]	101±1[3]	16.5±0.2	19.8±0.1	32.5±0.1	2.53

[a]Calculated by Guinier approximation; [b]Fitted with the sphere form factor. Different numbers in superscript denote statistical difference at $p < 0.05$.

Effects of BV and BV-Zn^{2+} complex on the pressure stability of apoMb

We employed fluorescence spectroscopy to study the effects of BV and its complex with Zn^{2+} ions on apoMb stability at *in situ* HP conditions. An increase in pressure induces a significant red shift of emission maximum from 333 nm at atmospheric pressure to 340-342 nm at 320 MPa, either in presence, or in absence of ligands (Figs. 4 and S8). This shift indicates exposing Trp and Tyr residues to solvent by pressure increase, which confirms the unfolding of apoMb (Fig. 4A). However, the pressure-induced red shift of emission spectra is significantly inhibited in presence of BV (Fig. 4B). At the same time, adding Zn^{2+} to BV exhibits more pronounced inhibitory effects (Fig. 4, C-D). Denaturation curves, obtained by monitoring the dependence of spectral shift on pressure, clearly demonstrate higher pressure stability of apoMb in presence of BV. Moreover, the addition of Zn^{2+} induces a more pronounced stabilisation effect (Table 2) with the increase of transition pressure ($P_{1/2}$) of ~110 MP, compared to the free apoMb. The obtained curves are well fitted into a two-state model (Eq. 14) and two thermodynamic parameters can be extracted: the unfolding volume change (ΔV_u) and Gibbs free energy change ($\Delta G_{0.1\ MPa}$). Calculated thermodynamic parameters for free apoMb

(Table 2) are in good agreement with previous studies based on HP fluorescence [42]. We observed that ΔV_u decreases in the following order: apoMb > apoMb-BV > apoMb-BV-Zn^{2+}. On the other hand, $\Delta G_{0.1\ MPa}$ increases in presence of BV or BV-Zn^{2+} complex (Table 2), indicating that apoMb-ligand complexes are more stable at atmospheric pressure in comparison to free protein.

Interestingly, the apoMb fluorescence intensity on pressure strongly depends on the presence of BV or BV-Zn^{2+} complex: in absence of ligands, the variation of fluorescence intensity at different pressures does not exceed 10% (Fig. 4A), while in presence of both BV and BV-Zn^{2+} complex, pressure increases protein fluorescence by 3-4 times (Figs. 4B, 4C and S9). This phenomenon can be ascribed to the dissociation of protein-ligand complexes during apoMb unfolding, while the dissociated ligand cannot quench apoMb fluorescence anymore, which induces the increase of protein fluorescence.

After HP treatment, up to 320 MPa (for free apoMb and apoMb-BV complex) and 380 MPa (for apoMb-BV-Zn^{2+} complex), the return to atmospheric pressure enables apoMb to refold either in the presence or the absence of ligands, but not entirely: the emission maximum is observed at around 334-335 nm for all samples (Fig. 4, A-C, doted lines). However, the observed emission maximum is much closer to the maximum of folded (333 nm) than the unfolded state (340-342 nm), suggesting that the pressure decrease may induce the apoMb native-like folding.

Effects of Zn^{2+} ions on the dissociation of apoMb-BV complex under HP

The presence of apoMb significantly shifts the VIS absorption peak of BV from 665 to 705 nm due to the conformational change of the BV chromophore upon binding to protein (Fig. 5A) [19]. Interestingly, the presence of Zn^{2+} ions induces the additional red shift of the VIS absorption peak of the apoMb-BV complex. We observed an absorption maximum of apoMb-BV-Zn^{2+} complex at 815 nm with a shoulder at 750 nm (Fig. 5B). The Zn^{2+} ions do not influence the absorption spectrum of

335 BV in absence of apoMb (data not shown), suggesting that Zn^{2+} ions could provoke BV
336 conformational change only when the pigment is bound to the protein.

337 ApoMb-BV complex exhibits good pressure stability up to 120 MPa, while further increase of
338 pressure induces a significant blue shift of BV chromophore, approaching the position absorption
339 maximum of the free chromophore at 240 MPa (Figs. 5A and S10). Hence, the obtained absorption
340 data confirm fluorescence results, *i.e.* that pressure triggers the dissociation of apoMb-BV complex.
341 On the other hand, the presence of Zn^{2+} ions strongly enhances the pressure stability of the apoMb-
342 BV complex and dissociation starts above 200 MPa (Fig. 5 B-C), followed by the decrease of peak
343 intensity at 815 nm. In contrast, above this pressure, the peak at 660-670 nm, arising from free BV,
344 starts to appear and increases up to the highest absorbance at 420 MPa. Based on the dependence of
345 absorbance ratio at 705 nm/665 nm and 815nm/665 nm upon pressure for apoMb-BV and apoMb-
346 BV-Zn^{2+} complex, respectively, we constructed the dissociation curves of apoMb-ligand complex.
347 Unambiguously, they confirm the higher pressure stability of apoMb-BV-Zn^{2+} complex with an
348 increase of the transition pressure ($P_{1/2}$) of ~100 MPa in comparison to apoMb-BV complex (Fig. 5C,
349 Table 2). Although the extracted thermodynamic parameters are somewhat different (both ΔV_u and
350 $\Delta G_{0.1MPa}$ are higher in absorption VIS measurements of BV spectra) in comparison to fluorescence
351 data obtained by excitation of aromatic side chains in apoMb, the trend in both techniques is the same:
352 ΔV_u decreases in presence of Zn^{2+}, while $\Delta G_{0.1MPa}$ for both samples does not differ significantly
353 (Table 2).

354 After HP treatment, up to 330 MPa (for free apoMb and apoMb-BV complex) and 420 MPa (for
355 apoMb-BV-Zn^{2+} complex), return to atmospheric pressure enables re-association of apoMb-BV
356 complex, as observed from the VIS absorption spectra of BV. Although apoMb-BV and apoMb-BV-
357 Zn^{2+} complexes exhibit quite different VIS absorption spectra before HP treatment, both complexes
358 have an absorption peak between 700 and 710 nm after HP treatment, corresponding to the absorption
359 maxima of apoMb-BV complex in absence of Zn^{2+} ions (Fig. 5, A-B). Therefore, HP treatment seems

to induce irreversible changes in the heme binding pocket of the apoMb structure, which disables the binding of the BV-Zn^{2+} complex to apoMb. Hence, only free BV can interact with apoMb (Fig. 5A) after HP treatment.

Table 2. Thermodynamic parameters of pressure behaviour of apoMb samples obtained from HP-VIS absorption and HP-fluorescence spectroscopy at pH 6.0.

Samples	Fluorescence[a]			Absorption[b]		
	ΔV_u (mL/mol)	$P_{1/2}$ (MPa)	$\Delta G_{0.1\ MPa}$ (kJ/mol)	ΔV_u (mL/mol)	$P_{1/2}$ (MPa)	$\Delta G_{0.1\ MPa}$ (kJ/mol)
apoMb	-77 ± 4	112 ± 2	8.6 ± 0.5	NA	NA	NA
apoMb-BV	-67 ± 3	184 ± 2	12.4 ± 0.6	-134 ± 6	198 ± 1	26±1
apoMb-BV-Zn^{2+}	-52 ± 4	244 ± 4	13± 1	-98 ± 6	290 ± 2	28±2

[a]Derived from the red shift of the emission peak of aromatic side chains (mainly Trp) within apoMb;

[b]Derived from the shift of the VIS peak of BV.

DISCUSSION

In the present study, we report that BV and BV-Zn^{2+} complex bind to apoMb with high affinity at the same binding site, while the presence of Zn^{2+} increases the BV binding constant. Both BV and BV-Zn^{2+} complexes make the apoMb structure more compact. In this context, BV significantly increases the pressure stability of apoMb. Moreover, the presence of Zn^{2+} ions substantially enhances the stabilisation effect of BV on apoMb structure at HP conditions.

The protein intrinsic fluorescence quenching approach reveals the ability of BV to interact with apoMb with high affinity, while the presence of Zn^{2+}ions induces a slight increase of BV binding constant to protein. On the other hand, no significant quenching of apoMb fluorescence is observed due to Zn^{2+} ions in absence of BV (data not shown). Interestingly, previous studies demonstrated the ability of heme to displace the BV from the apoMb binding pocket, but heme-induced displacement could not be observed when the complex of BV analogue (meso-BV) with Zn^{2+} is bound to apoMb

[24]. The higher stability of the apoMb-BV complex in presence of Zn^{2+} and the larger binding constant obtained in our study could be explained by additional interactions of Zn^{2+} with the proximal His93 residue, oriented toward tetrapyrrole chromophore in the heme binding pocket [24, 30]. Indeed, the present molecular docking study revealed the close proximity of Zn^{2+} ions with His93, and their proper orientation towards each other makes the formation of coordination bond highly possible. This makes apoMb-BV-Zn^{2+} complex less sensitive to dissociation in comparison to the complex in absence of Zn^{2+} ions.

CD spectroscopy and SAXS measurements revealed the ability of BV to induce conformational changes in apoMb. Both BV and BV-Zn^{2+} complex binding not only increases the α-helical content in apoMb but also triggers the formation of coil-coil structures, making the protein structure more compact. We also observed by SAXS measurements a decrease of R_g and volume of apoMb upon ligand binding, additionally confirming higher compactness of both apoMb-BV and apoMb-BV-Zn^{2+} complexes. Interestingly, holoMb also has significantly higher α-helical content and compactness than the apo form of the protein [43, 44], suggesting that apoMb-BV complex, either in presence, or in absence of Zn^{2+} ions, has high structural similarity to holoMb. Indeed, the comparison of the crystal structures of holoMb and apoMb-BV complex confirms these findings [30, 45]. Therefore, BV mimics the heme in its biding site, inducing the conformational change of apoMb towards a more rigid structure.

An increase of pressure up to 320 MPa induces the unfolding of apoMb, as observed by the shift of emission maxima from 333 to 341 nm. However, previous studies revealed that the complete unfolding of apoMb comprises the shift of the emission maximum to 355 nm, indicating that HP only partially unfolds apoMb [46]. Indeed, Tanaka & al. [43] demonstrated that pressure values up to 400 MPa could disintegrate the part of apoMb that contains the heme binding site, but without the ability to unfold the complete protein. The binding of BV and BV-Zn^{2+} complex significantly increases the pressure stability of apoMb, as concluded by the substantial shift of the half-transition point ($P_{1/2}$).

Moreover, extrapolated $\Delta G_{0.1\ MPa}$ values confirm higher stability of apoMb-ligand complexes at atmospheric pressure, which is in accordance with the CD and SAXS measurements described above. The presence of Zn^{2+} ions significantly enhances the stabilisation effect of BV on apoMb structure at HP conditions, probably through additional interaction of metal ions with the amino acid side chains in the heme binding pocket. It is well known that His93 coordinates to Fe in holoMb [45], and considering the ability of BV to mimic the heme in its binding pocket, the interaction of Zn^{2+} within His93 is highly possible [24], as shown by the molecular docking experiment in the present study. Moreover, it is well known that holoMb has significantly higher pressure stability than apoMb [47]. Besides, there is no effect of Zn^{2+} on pressure stability of apoMb in absence of BV (data not shown), confirming that only Zn^{2+} bound to BV could provoke a higher stabilisation of apoMb structure at HP conditions.

The observed volume change of 77 mL/mol for apoMb without ligands is comparable to volume changes (53-106 mL/mol) obtained by HP-NMR and HP-fluorescence studies [42, 43, 48]. For all samples, the calculated ΔV_u are negative, probably indicating two phenomena: *i*) a HP-induced increase of the hydration of apoMb heme binding pocket [49-51] and *ii*) the electrostriction of water molecules may interact with the negative charges of apoMb residues exposed to the solvent by the protein unfolding [52]. The decrease of ΔV_u upon pressure for apoMb-ligand complexes, especially for the apoMb-BV-Zn^{2+} one, in comparison to free apoMb, may also be explained by a larger initial volume of uncomplexed protein at atmospheric pressure. Volume calculation of apoMb, holoMb, and apoMb-BV crystal structures showed an increase in the total volume of unliganded apoMb of 2 and 4% compared to apoMb-BV complex and holoMb, respectively [53]. Moreover, the protein volume determined in this study by SAXS measurements confirms a larger volume of free apoMb compared to the apoMb-BV and apoMb-BV-Zn^{2+} complexes (see V values in Table 1).

Interestingly, the HP-fluorescence study reveals that apoMb-BV and apoMb-BV-Zn^{2+} complex dissociation is simultaneous with the protein unfolding, which is in agreement with the observation that HP manifests its effects on apoMb structure through the disintegration of heme binding pocket.

The significant red shift of the VIS absorption peak of the BV chromophore upon binding to apoMb is a valuable phenomenon to study the effects of HP on the dissociation of apoMb-BV complex. The obtained red shift of bound BV could be ascribed to the flattening or compression of the BV helicoidal cyclic conformation, as confirmed by crystallographic and NMR studies [30, 54]. The BV molecule binds in the heme pocket, making the overall molecular shape as "similar to the heme" as possible. Therefore, the helical conformation of BV has a minimal helix pitch in order to mimic the flat heme conformation in the protein binding pocket [30]. However, the BV conformation in the bound state is still not completely flat (~3Å helical pitch), while the iron coordination of four pyrrole rings makes heme mostly completely flat in the myoglobin binding site [30]. In this context, the presence of Zn^{2+} within the apoMb-BV complex induces an additional red shift in BV absorption spectra, which could be explained by the more pronounced compression of BV helix through coordination of Zn^{2+} ions with the nitrogen of pyrrole rings of BV [24]. Hence, the addition of Zn^{2+} ions makes the apoMb-BV complex more rigid, which is confirmed by the *in situ* HP-VIS absorption study: Zn^{2+} increases the transition point ($P_{1/2}$) of the apoMb-BV complex by almost 100 MPa. Additionally, the volume change of dissociation of the apoMb-BV complex is lower in presence of Zn^{2+} ions, which is in accordance with the *in situ* HP-fluorescence study. Moreover, as described above, the initial volume of the apoMb-BV complex is larger than the heme-bound Mb crystal structure (holoMb) [30, 45, 53], suggesting that metal-bound tetrapyrrole makes the binding pocket within apoMb more compact. Meanwhile, no Zn^{2+}-induced red shift in the absorption spectrum of BV is observed in absence of protein, indicating that initial, apoMb-triggered flattening of BV helicoidal conformation is a prerequisite for Zn^{2+} to compress BV chromophore.

However, the thermodynamic parameters (ΔV_u, $\Delta G_{0.1\ MPa}$, $P_{1/2}$) of both apoMb-BV and apoMb-BV-Zn^{2+} complexes obtained by HP-VIS absorption spectroscopy of BV chromophore are substantially higher in comparison to the HP-fluorescence measurements of apoMb aromatic side chains. These differences could be explained by: *i*) ten times higher concentration of protein-ligand complex in absorption experiments inhibits the apoMb-BV dissociation (either in presence, or in absence of Zn^{2+}) inducing the increase of $P_{1/2}$ compared to the HP-fluorescence measurements; and *ii*) absorption measurements reveal only the change of environment of BV chromophore at HP conditions and thermodynamic parameters obtained by this approach are strongly related with the BV binding pocket within apoMb. On the other hand, the pressure-induced fluorescence changes of aromatic side chains reflect not only the behavior of the BV binding site but also other regions, including the N-terminus where Trp residues (the major contributors of apoMb fluorescence) are located [30]. Therefore, the BV chromophore is a valuable probe that can provide thermodynamic parameters specifically related to the behavior of the hydrophobic pocket within apoMb at HP.

The high-pressure unfolding of apoMb, either in absence, or in presence of BV or BV-Zn^{2+} complex, is mostly reversible (> 85%, based on the position of emission maximum) but not entirely. Interestingly, apoMb-BV complex is fully recovered after HP treatment, suggesting that the apoMb binding pocket is well refolded. However, HP treatment disables reassociation of apoMb-BV-Zn^{2+} complex after HP treatment: pressurisation of apoMb-BV-Zn^{2+} complex, followed by pressure decrease, induces the formation of apoMb-BV complex without Zn^{2+} bound to the protein-ligand complex. Therefore, it seems that pressure causes subtle structural rearrangements within the apoMb binding pocket, which disables the interactions of Zn^{2+} with the amino acid side chains, crucial for the tight anchoring of Zn^{2+} within the apoMb-BV complex. Indeed, Lerch *et al.* revealed that HP induces the movement of Fe-interacting residue (His93) within holoMb [47], indicating that rearrangement of this residue is responsible for the inability of Zn^{2+} to interact with apoMb-BV complex after HP treatment.

CONCLUSIONS

We report here the effects of two ligands, BV and BV-Zn^{2+} complex, on the structure and pressure stability of apoMb, by combining CD, SAXS, *in situ* HP-fluorescence and HP-VIS absorption spectroscopies. BV binds to apoMb with high affinity, and the presence of Zn^{2+} enhances BV binding affinity. BV and BV-Zn^{2+} complex have the same binding site on apoMb. Both ligands induce conformational changes in apoMb, leading to the higher α-helical content and higher compactness of protein structure. The binding of BV to the apoMb hydrophobic pocket strongly stabilises the protein at HP. Coordination of Zn^{2+} to BV within apoMb, makes helicoidal conformation of tetrapyrrole chromophore compressed and enables additional interactions of the metal ion with amino acid residues in the hydrophobic protein pocket, which enhances the pressure stability of the protein. The return to atmospheric pressure after HP treatment induces refolding of apoMb with the complete ability to bind BV. However, HP treatment irreversible causes subtle conformational changes in apoMb, disabling interactions of Zn^{2+} with amino acid residues within the protein binding pocket and consequently preventing its coordination to apoMb-bound BV. More generally, our results highlight the stabilisation mechanism of the hydrophobic pocket within apoMb, which is crucial for the successful transportation and delivery of bioactive molecules by apoMb.

AUTHOR CONTIRUBTIONS

SM, AB, and SC designed research; SM, AB, and SC conducted *in vitro* experiments; MM conducted docking experiments; BA and FM provided expertise and technical support for high pressure experiments; SM, MM, AB and SC analysed data and wrote the paper.

FIGURE CAPTIONS

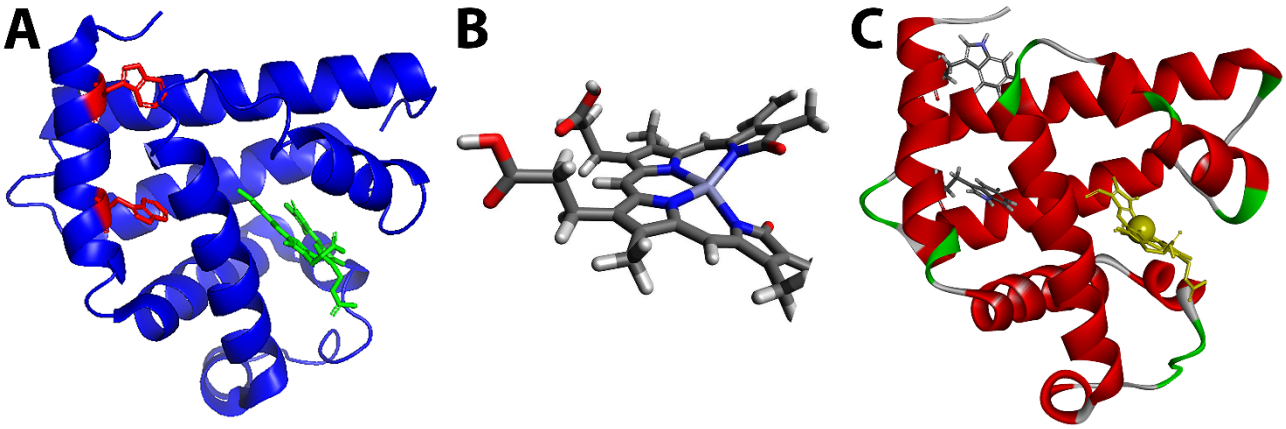

Figure 1. (*A*) Ribbon model of the crystal structure of apoMb (PDB:1BVC) in complex with BV. Tryptophan (Trp) aromatic side chains and BV are shown in red (Trp7 and Trp14) and green color, respectively; (*B*) Optimised structure of BV-Zn^{2+} complex. Zn, nitrogen, oxygen, carbon, and hydrogen atoms are shown in light purple, blue, red, dark grey, and light grey colours, respectively; (*C*) BV-Zn^{2+} complex (in yellow) docked in the heme binding pocket of apoMb. Trp7 and Trp14 are shown in grey stick representation.

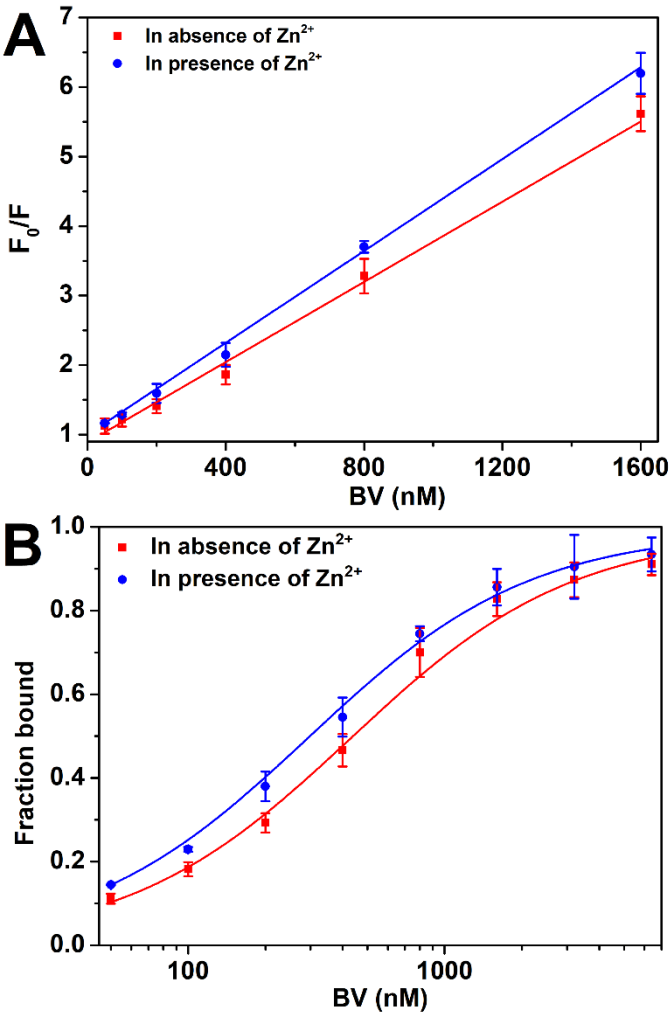

505

506 **Figure 2.** (*A*) Stern–Volmer plots of apoMb fluorescence quenched by BV and BV-Zn^{2+} complex at
507 pH 6.0 and 20 °C; (*B*) Fluorescence quenching-based binding curves for BV interaction to apoMb in
508 presence (red circles) and in absence (black squares) of Zn^{2+}.

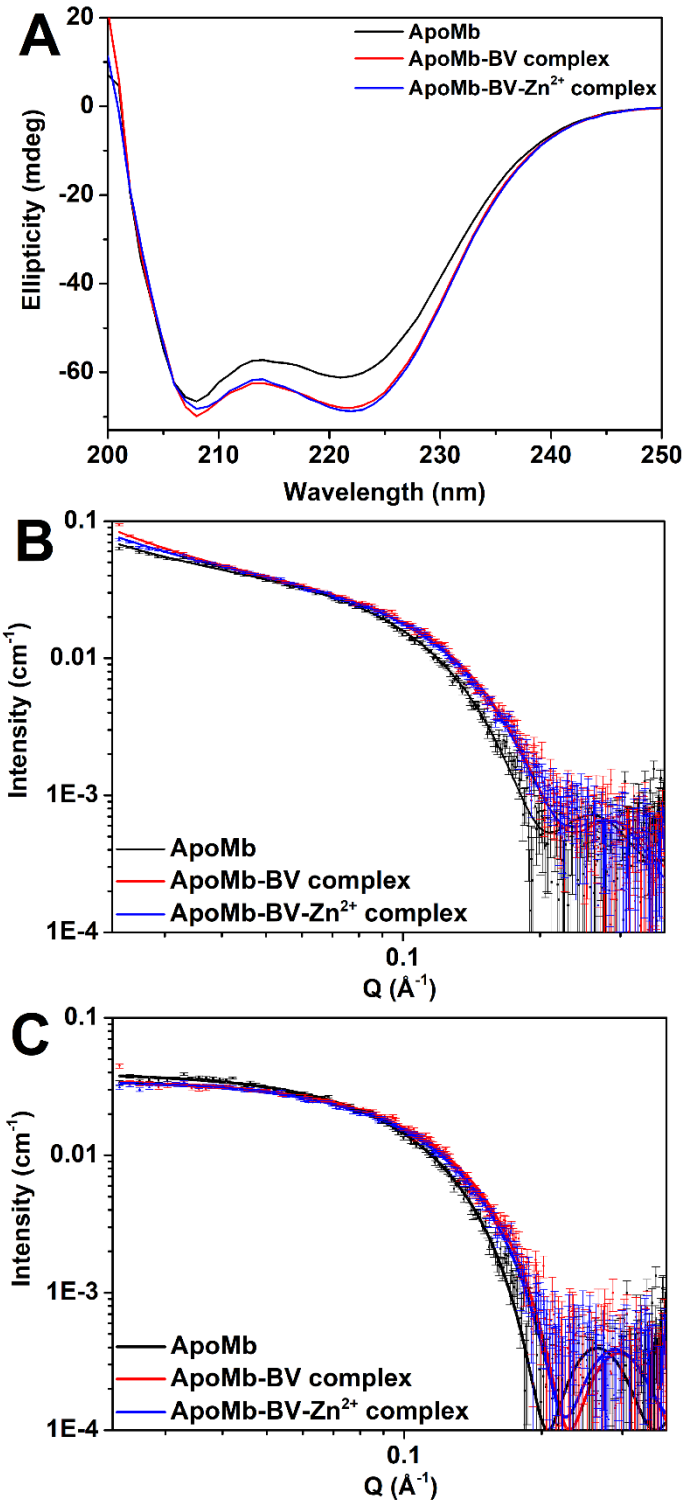

509

510 **Figure 3.** (*A*) Far-UV CD spectra of apoMb (10 μM) in absence and in presence of BV (10 μM) or
511 BV-Zn^{2+} complex (10 μM BV, 100 μM Zn^{2+}); (*B*) SAXS intensities of apoMb (235 μM) in presence
512 of BV (235 μM) or BV-Zn^{2+} complex (235 μM both).

513

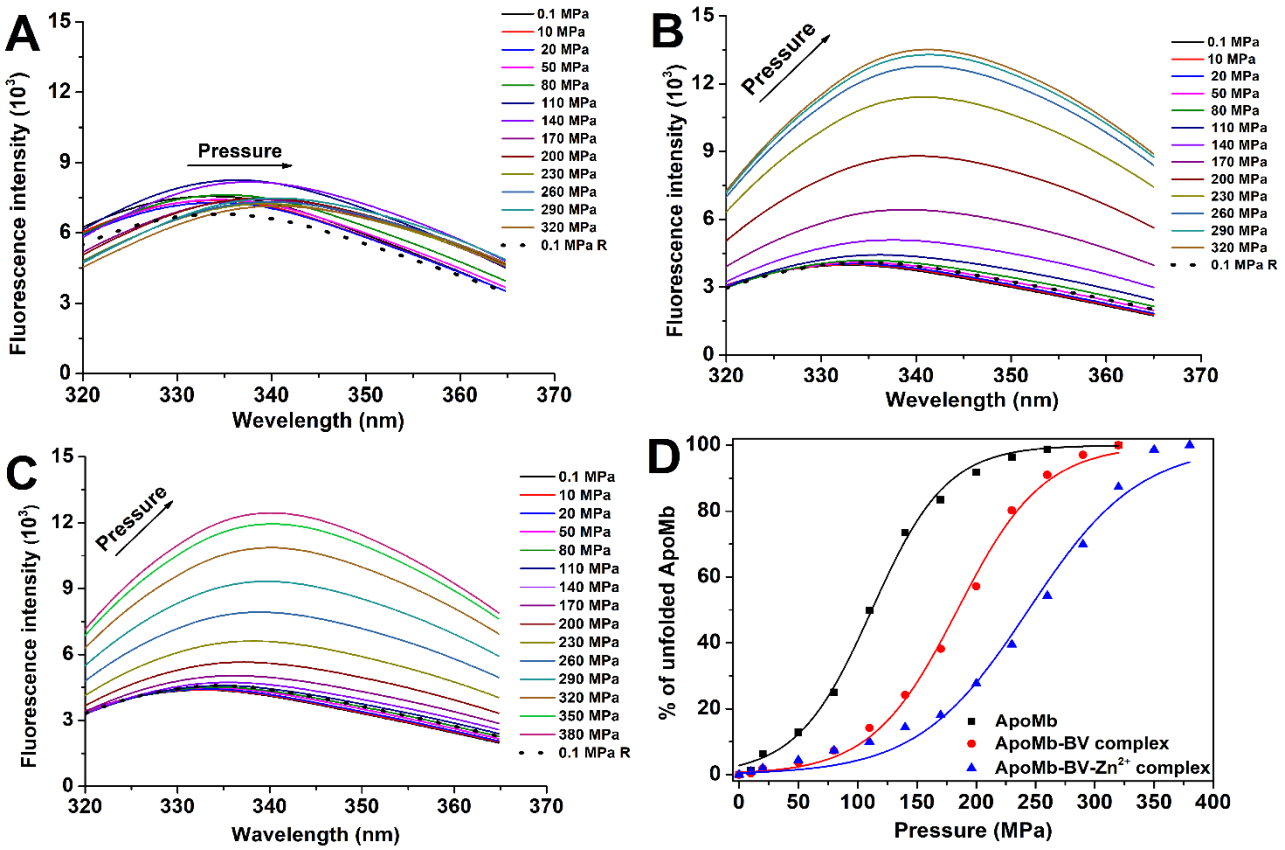

514

515 **Figure 4.** *In situ* HP fluorescence measurements (excitation at 280 nm) of apoMb (10 μM) (*A*) in
516 absence and in presence of (*B*) BV (10 μM) or (*C*) BV-Zn^{2+} complex (10 μM BV, 100 μM Zn^{2+}).
517 The dotted line represents the fluorescence spectra of apoMb in absence (*A*) and absence of ligands
518 (*B* and *C*) after coming back to 0.1 MPa. (*D*) Percentage of unfolded apoMb (Eq. 13) and the
519 corresponding unfolding fits (full lines, Eq. 14) are shown as a function of pressure in absence or in
520 presence of BV or BV-Zn^{2+} complex.

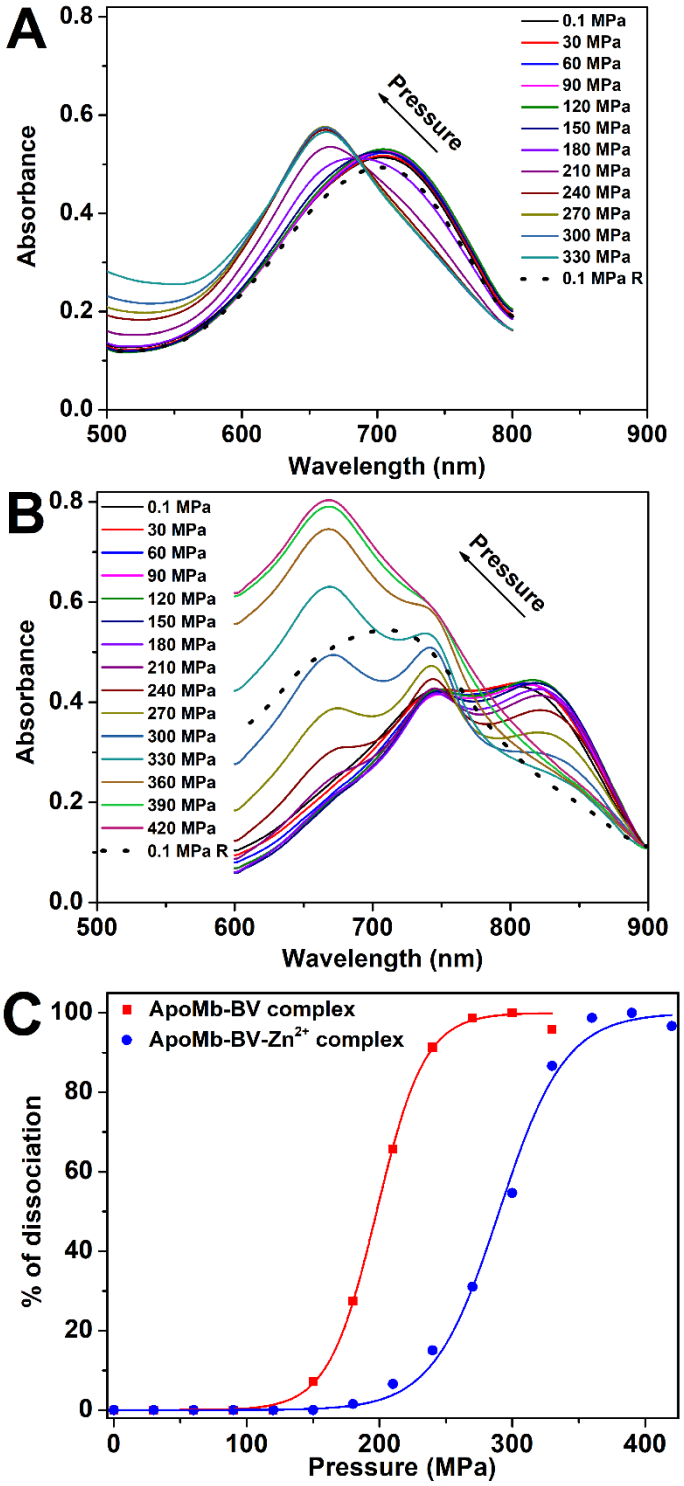

521

522 **Figure 5.** *In situ* HP-VIS absorption measurements of apoMb (80 µM) in presence of (*A*) BV (80
523 µM) or (*B*) BV-Zn^{2+} complex (80 µM BV, 80 µM Zn^{2+}). The dotted line represents the absorption
524 spectra of apoMb in absence (*A*) and presence of Zn^{2+} (*B*) after coming back to 0.1 MPa. (*C*)
525 Percentage of dissociated apoMb-ligand complex (Eq. 13) and the corresponding unfolding fits (full
526 lines, Eq. 14) as a function of pressure in presence of BV or BV-Zn^{2+} complex.

REFERENCES

[1] I. Pal, M. Roy, S.G. Dey, Interaction of ApoMyoglobin with Heme-hIAPP complex, J Inorg Biochem 216 (2021) 111348. https://doi.org:10.1016/j.jinorgbio.2020.111348.

[2] P. Picotti, A. Marabotti, A. Negro, V. Musi, B. Spolaore, M. Zambonin, A. Fontana, Modulation of the structural integrity of helix F in apomyoglobin by single amino acid replacements, Protein Sci 13(6) (2004) 1572-85. https://doi.org:10.1110/ps.04635304.

[3] N. Taulier, I.V. Beletskaya, T.V. Chalikian, Compressibility changes accompanying conformational transitions of apomyoglobin, Biopolymers 79(4) (2005) 218-29. https://doi.org:10.1002/bip.20350.

[4] R. Mohana-Borges, N.K. Goto, G.J. Kroon, H.J. Dyson, P.E. Wright, Structural characterisation of unfolded states of apomyoglobin using residual dipolar couplings, J Mol Biol 340(5) (2004) 1131-42. https://doi.org:10.1016/j.jmb.2004.05.022.

[5] M. Cozzolino, L. Pesce, D. Pezzuoli, C. Montali, L. Brancaleon, L. Cavanna, S. Abbruzzetti, A. Diaspro, P. Bianchini, C. Viappiani, Apomyoglobin is an efficient carrier for zinc phthalocyanine in photodynamic therapy of tumors, Biophys Chem 253 (2019) 106228. https://doi.org:10.1016/j.bpc.2019.106228.

[6] I.S. Pires, Q.T. O'Boyle, C.J. Munoz, C. Savla, P. Cabrales, A.F. Palmer, Enhanced Photodynamic Therapy Using the Apohemoglobin-Haptoglobin Complex as a Carrier of Aluminum Phthalocyanine, ACS Appl Bio Mater 3(7) (2020) 4495-4506. https://doi.org:10.1021/acsabm.0c00450.

[7] D. Zhang, R. Lazim, Application of conventional molecular dynamics simulation in evaluating the stability of apomyoglobin in urea solution, Sci Rep 7 (2017) 44651. https://doi.org:10.1038/srep44651.

[8] J. Roche, J.A. Caro, D.R. Norberto, P. Barthe, C. Roumestand, J.L. Schlessman, A.E. Garcia, B.E. Garcia-Moreno, C.A. Royer, Cavities determine the pressure unfolding of proteins, Proc Natl Acad Sci U S A 109(18) (2012) 6945-50. https://doi.org:10.1073/pnas.1200915109.

[9] S. Minic, B. Annighofer, A. Helary, D. Hamdane, G. Hui Bon Hoa, C. Loupiac, A. Brulet, S. Combet, Effect of Ligands on HP-Induced Unfolding and Oligomerization of beta-Lactoglobulin, Biophys J 119(11) (2020) 2262-2274. https://doi.org:10.1016/j.bpj.2020.10.019.

[10] Z. Toleikis, P. Cimmperman, V. Petrauskas, D. Matulis, Determination of the volume changes induced by ligand binding to heat shock protein 90 using high-pressure denaturation, Anal Biochem 413(2) (2011) 171-8. https://doi.org:10.1016/j.ab.2011.02.019.

[11] G. Skvarnavicius, Z. Toleikis, D. Matulis, V. Petrauskas, Denaturant- or ligand-induced changes in protein volume by pressure shift assay, Phys Chem Chem Phys 24(28) (2022) 17279-17288. https://doi.org:10.1039/d2cp01046a.

[12] B. Pucelik, A. Sułek, J.M. Dąbrowski, Bacteriochlorins and their metal complexes as NIR-absorbing photosensitisers: properties, mechanisms, and applications, Coord Chem Rev 416 (2020). https://doi.org:10.1016/j.ccr.2020.213340.

[13] K.B. Singh, Kaushalendra, J.P. Rajan, Therapeutical and Nutraceutical Roles of Cyanobacterial Tetrapyrrole Chromophore: Recent Advances and Future Implications, Front Microbiol 13 (2022) 932459. https://doi.org:10.3389/fmicb.2022.932459.

[14] L.A. Kasatkina, C. Ma, M.E. Matlashov, T. Vu, M. Li, A.A. Kaberniuk, J. Yao, V.V. Verkhusha, Optogenetic manipulation and photoacoustic imaging using a near-infrared transgenic mouse model, Nat Commun 13(1) (2022) 2813. https://doi.org:10.1038/s41467-022-30547-6.

[15] I. Sóvágó, B. Harman, I. Kolozsvári, F. Matyuska, Complex-formation and redox reactions of bilirubin and biliverdin with zinc(II), cadmium(II) and copper(II) ions, Inorganica Chim Acta 106(4) (1985) 181-186. https://doi.org/10.1016/S0020-1693(00)82266-5.

[16] N. Plekhova, O. Shevchenko, O. Korshunova, A. Stepanyugina, I. Tananaev, V. Apanasevich, Development of Novel Tetrapyrrole Structure Photosensitizers for Cancer Photodynamic Therapy, Bioengineering (Basel) 9(2) (2022). https://doi.org:10.3390/bioengineering9020082.

[17] T. Jansen, A. Daiber, Direct Antioxidant Properties of Bilirubin and Biliverdin. Is there a Role for Biliverdin Reductase?, Front Pharmacol 3 (2012) 30. https://doi.org:10.3389/fphar.2012.00030.

[18] C.T. Beuckmann, M. Aoyagi, I. Okazaki, T. Hiroike, H. Toh, O. Hayaishi, Y. Urade, Binding of biliverdin, bilirubin, and thyroid hormones to lipocalin-type prostaglandin D synthase, Biochemistry 38(25) (1999) 8006-13. https://doi.org:10.1021/bi990261p.

[19] H. Marko, N. Miiller, H. Falk, Complex Formation Between Biliverdin and Apomyoglobin, Monatsh Chem 120 (1989) 591-595.

[20] Y.L. Wei, J.Q. Li, C. Dong, S.M. Shuang, D.S. Liu, C.W. Huie, Investigation of the association behaviors between biliverdin and bovine serum albumin by fluorescence spectroscopy, Talanta 70(2) (2006) 377-82 . https://doi.org:10.1016/j.talanta.2006.02.052.

583 [21] M.S. Dimitrijevic, J. Bogdanovic Pristov, M. ziZic, D.M. Stankovic, D. Bajuk-Bogdanovic, M. Stanic, S.
584 Spasic, W. Hagen, I. Spasojevic, Biliverdin-copper complex at physiological pH, Dalton Trans 48(18) (2019)
585 6061-6070. https://doi.org:10.1039/c8dt04724c.
586 [22] J. Kolsenik, B. Belgorodsky, L. Fadeev, M. Gozin, Can apomyoglobin form a complex with a spherical
587 ligand? Interactions between apomyoglobin and [C60] fullerene derivative, J Nanosci Nanotechnol 7(4-5)
588 (2007) 1389-94. https://doi.org:10.1166/jnn.2007.318.
589 [23] P. Bianchini, M. Cozzolino, M. Oneto, L. Pesce, F. Pennacchietti, M. Tognolini, C. Giorgio, S. Nonell,
590 L. Cavanna, P. Delcanale, S. Abbruzzetti, A. Diaspro, C. Viappiani, Hypericin-Apomyoglobin: An Enhanced
591 Photosensitizer Complex for the Treatment of Tumor Cells, Biomacromolecules 20(5) (2019) 2024-2033.
592 https://doi.org:10.1021/acs.biomac.9b00222.
593 [24] H. Falk, H. Marko, N. Miiller, W. Schmitzberger, On the Chemistry of Pyrrole Pigments, LXXXVII [1]:
594 The Apomyoglobin Heme Pocket as a Reaction Vessel in Bile Pigment Chemistry, Monatsh Chem 121 (1990)
595 903-908.
596 [25] L. Luo, C.H. Chang, Y.C. Chen, T.K. Wu, E.W. Diau, Ultrafast relaxation of zinc protoporphyrin
597 encapsulated within apomyoglobin in buffer solutions, J Phys Chem B 111(26) (2007) 7656-64.
598 https://doi.org:10.1021/jp068449n.
599 [26] Y. Kawamura-Konishi, H. Kihara, H. Suzuki, Reconstitution of myoglobin from apoprotein and heme,
600 monitored by stopped-flow absorption, fluorescence and circular dichroism, Eur J Biochem 170(3) (1988)
601 589-95. https://doi.org:10.1111/j.1432-1033.1988.tb13738.x.
602 [27] J.R. Lakowicz, Principles of Fluorescence Spectroscopy, Springer, New York, 2006.
603 [28] J.M. Glandieres, C. Twist, A. Haouz, C. Zentz, B. Alpert, Resolved fluorescence of the two tryptophan
604 residues in horse apomyoglobin, Photochem Photobiol 71(4) (2000) 382-6. https://doi.org:10.1562/0031-
605 8655(2000)071<0382:rfottt>2.0.co;2.
606 [29] J.K. Keppler, M.C. Stuhldreier, F. Temps, K. Schwarz, Influence of mathematical models and correction
607 factors on binding results of polyphenols and retinol with β-lactoglobulin measured with fluorescence
608 quenching, Food Biophysics 9(2) (2014) 158-168. https://doi.org:10.1007/s11483-013-9328-x.

609 [30] U.G. Wagner, N. Muller, W. Schmitzberger, H. Falk, C. Kratky, Structure determination of the biliverdin
610 apomyoglobin complex: crystal structure analysis of two crystal forms at 1.4 and 1.5 A resolution, J Mol Biol
611 247(2) (1995) 326-37. https://doi.org:10.1006/jmbi.1994.0142.
612 [31] G.M. Morris, R. Huey, W. Lindstrom, M.F. Sanner, R.K. Belew, D.S. Goodsell, A.J. Olson, AutoDock4
613 and AutoDockTools4: Automated Docking with Selective Receptor Flexiblity, J Comput. Chem. 30 (2009)
614 2785–91 http://dx.doi.org/10.1002/jcc.21256
615 [32] I. Matei, M. Hillebrand, Interaction of kaempferol with human serum albumin: a fluorescence and circular
616 dichroism study, J Pharm Biomed Anal 51(3) (2010) 768-73. https://doi.org:10.1016/j.jpba.2009.09.037.
617 [33] Y. Wei, A.A. Thyparambil, R.A. Latour, Protein helical structure determination using CD spectroscopy
618 for solutions with strong background absorbance from 190 to 230 nm, Biochim Biophys Acta 1844(12) (2014)
619 2331-7. https://doi.org:10.1016/j.bbapap.2014.10.001.
620 [34] A. Brûlet, D. Lairez, A. Lapp, J.-P. Cotton, Improvement of data treatment in small-angle neutron
621 scattering, J Appl Crystallogr 40(1) (2007) 165-177. https://doi.org:10.1107/s0021889806051442.
622 [35] A. Guinier, G. Fournet, Small angle scattering of X-rays, John Wiley & Sons, INC, New York, 1955.
623 [36] P.V. Konarev, V.V. Volkov, A.V. Sokolova, M.H.J. Koch, D.I. Sverguna, PRIMUS: a Windows PC-
624 based system for smallangle scattering data analysis J Appl Crystallogr 36 (2003) 1277-1282.
625 https://doi.org:10.1107/S0021889803012779
626 [37] E. Dufour, G.H. Hoa, T. Haertle, High-pressure effects on beta-lactoglobulin interactions with ligands
627 studied by fluorescence, Biochim Biophys Acta 1206(2) (1994) 166-72. https://doi.org:10.1016/0167-
628 4838(94)90204-6.
629 [38] R. Lange, N. Bec, V.V. Mozhaev, J. Frank, Fourth derivative UV-spectroscopy of proteins under high
630 pressure II. Application to reversible structural changes, Eur Biophys J 24 (1996) 284-292.
631 [39] S. Minic, B. Annighofer, A. Helary, L. Sago, D. Cornu, A. Brulet, S. Combet, Structure of proteins under
632 pressure: Covalent binding effects of biliverdin on beta-lactoglobulin, Biophys J 121(13) (2022) 2514-2525.
633 https://doi.org:10.1016/j.bpj.2022.06.003.
634 [40] S.L. Minic, M. Milcic, D. Stanic-Vucinic, M. Radibratovic, T.G. Sotiroudis, M.R. Nikolic, T.Ć.
635 Velickovic, Phycocyanobilin, a bioactive tetrapyrrolic compound of blue-green alga Spirulina, binds with high

affinity and competes with bilirubin for binding on human serum albumin, RSC Advances 5(76) (2015) 61787-61798. https://doi.org:10.1039/c5ra05534b.

[41] A. Lathbridge, J.M. Mason, Combining Constrained Heptapeptide Cassettes with Computational Design To Create Coiled-Coil Targeting Helical Peptides, ACS Chem Biol 14(6) (2019) 1293-1304. https://doi.org:10.1021/acschembio.9b00265.

[42] G.J. Vidugiris, C.A. Royer, Determination of the volume changes for pressure-induced transitions of apomyoglobin between the native, molten globule, and unfolded states, Biophys J 75(1) (1998) 463-70. https://doi.org:10.1016/S0006-3495(98)77534-4.

[43] N. Tanaka, C. Ikeda, K. Kanaori, K. Hiraga, T. Konno, S. Kunugi, Pressure effect on the conformational fluctuation of apomyoglobin in the native state, Biochemistry 39(39) (2000) 12063-8. https://doi.org:10.1021/bi001009g.

[44] F.M. Hughson, P.E. Wright, R.L. Baldwin, Structural characterisation of a partly folded apomyoglobin intermediate, Science 249(4976) (1990) 1544-8. https://doi.org:10.1126/science.2218495.

[45] S.V. Evans, G.D. Brayer, High-resolution study of the three-dimensional structure of horse heart metmyoglobin, J Mol Biol 213(4) (1990) 885-97. https://doi.org:10.1016/S0022-2836(05)80270-0.

[46] E. Bismuto, I. Sirangelo, G. Irace, E. Gratton, Pressure-induced perturbation of apomyoglobin structure: fluorescence studies on native and acidic compact forms, Biochemistry 35(4) (1996) 1173-8. https://doi.org:10.1021/bi951163g.

[47] M.T. Lerch, J. Horwitz, J. McCoy, W.L. Hubbell, Circular dichroism and site-directed spin labeling reveal structural and dynamical features of high-pressure states of myoglobin, Proc Natl Acad Sci U S A 110(49) (2013) E4714-22. https://doi.org:10.1073/pnas.1320124110.

[48] S.E. Bondos, S. Sligar, J. Jonas, High-pressure denaturation of apomyoglobin, Biochim Biophys Acta 1480(1-2) (2000) 353-64. https://doi.org:10.1016/s0167-4838(00)00088-1.

[49] C. Di Primo, G. Hui Bon Hoa, P. Douzou, S.G. Sligar, Heme-pocket-hydration change during the inactivation of cytochrome P-450camphor by hydrostatic pressure, Eur J Biochem 209(2) (1992) 583-8. https://doi.org:10.1111/j.1432-1033.1992.tb17323.x.

[50] G. Hui Bon Hoa, M.A. McLean, S.G. Sligar, High pressure, a tool for exploring heme protein active sites, Biochim Biophys Acta 1595(1-2) (2002) 297-308. https://doi.org:10.1016/s0167-4838(01)00352-1.

664 [51] J.A. Rupley, G. Careri, Protein hydration and function, Adv Protein Chem 41 (1991) 37-172.
665 https://doi.org:10.1016/s0065-3233(08)60197-7.
666 [52] C.A. Royer, Revisiting volume changes in pressure-induced protein unfolding, Biochim Biophys Acta
667 1595(1-2) (2002) 201-9. https://doi.org:10.1016/s0167-4838(01)00344-2.
668 [53] N.R. Voss, M. Gerstein, 3V: cavity, channel and cleft volume calculator and extractor, Nucleic Acids Res
669 38(Web Server issue) (2010) W555-62. https://doi.org:10.1093/nar/gkq395.
670 [54] H. Marko, N. Muller, H. Falk, Nuclear-magnetic-resonance investigations of the biliverdin-apomyoglobin
671 complex, Eur J Biochem 193(2) (1990) 573-80. https://doi.org:10.1111/j.1432-1033.1990.tb19374.x.